

Novel Interplay between High- T_c Superconductivity and Antiferromagnetism in Tl-based Six-CuO₂-Layered Cuprates: ²⁰⁵Tl- and ⁶³Cu-NMR Probes

Hidekazu Mukuda^{1*}, Nozomu Shiki¹, Naoki Kimoto¹, Mitsuharu Yashima¹, Yoshio Kitaoka¹, Kazuyasu Tokiwa², and Akira Iyo³

¹Graduate School of Engineering Science, Osaka University, Toyonaka, Osaka 560-8531, Japan

²Department of Applied Electronics, Science University of Tokyo, Noda, Chiba 278-8510, Japan

³National Institute of Advanced Industrial Science and Technology (AIST), Umezono, Tsukuba 305-8568, Japan

(Received June 28, 2016)

We report ⁶³Cu- and ²⁰⁵Tl-NMR studies on six-layered ($n=6$) high- T_c superconducting (SC) cuprate TlBa₂Ca₅Cu₆O_{14+δ} (Tl1256) with $T_c \sim 100$ K, which reveal that antiferromagnetic (AFM) order takes place below $T_N \sim 170$ K. In this compound, four underdoped inner CuO₂ planes ($n(\text{IP})=4$) sandwiched by two outer planes (OPs) are responsible for the onset of AFM order, whereas the nearly optimally-doped OPs responsible for the onset of bulk SC. It is pointed out that an increase in the out-of-plane magnetic interaction within an intra-unit-cell causes $T_N \sim 45$ K for Tl1245 with $n(\text{IP})=3$ to increase to ~ 170 K for Tl1256 with $n(\text{IP})=4$. It is remarkable that the marked increase in T_N and the AFM moments for the IPs does not bring about any reduction in T_c , since $T_c \sim 100$ K is maintained for both compounds with nearly optimally doped OP. We highlight the fact that the SC order for $n \geq 5$ is mostly dominated by the long-range in-plane SC correlation even in the multilayered structure, which is insensitive to the magnitude of T_N and the AFM moments at the IPs or the AFM interaction among the IPs. These results demonstrate a novel interplay between the SC and AFM orders when the charge imbalance between the IPs and OP is significantly large.

The parent materials of hole-doped high- T_c cuprates are antiferromagnetic (AFM) Mott insulators characterized by a large in-plane superexchange interaction $J_{\text{in}} \sim 1300$ K among the $S=1/2$ spins at the Cu sites. Since the theory demonstrates that no long-range order takes place at finite temperature for two-dimensional (2D) antiferromagnets,¹ the onset of AFM order is actually mediated by three-dimensional (3D) magnetic interactions such as $J_{\text{out}}(n)$ among the CuO₂ layers within an intra-unit-cell and J_{CRL} among an inter-unit-cell through the blocking charge reservoir layer (CRL). Note that $J_{\text{out}}(n)$ and J_{CRL} are much smaller than J_{in} . As a matter of fact, as the number of CuO₂ planes (n) increases in the unit cell, the Néel temperature (T_N) of 325 K for single-layered La₂CuO₄ ($n=1$) increases to 410 K for bilayered YBCO ($n=2$) and to 537 K for infinite-layered (Ca,Sr)CuO₂ ($n=\infty$); nevertheless the size of the AFM moment does not depend on n .²

Multilayered copper oxides TlBa₂Ca _{$n-1$} Cu _{n} O _{$2n+2+\delta$} (Tl12($n-1$) n) with $n \geq 3$ include two types of CuO₂ planes, an outer CuO₂ plane (OP) with fivefold oxygen coordination and an inner plane (IP) with fourfold coordination with no apical oxygen, as shown in Fig. 1(a). The hole density $p(\text{OP})$ is always larger than $p(\text{IP})$, since the OP is closer to the CRL than to the IPs. In other words, the spatially dependent Madelung potential for hole carriers from the apical oxygen O²⁻ becomes smaller as IPs are apart from the CRL.³⁻⁶ Accordingly, as n increases, the $p(\text{IP})$ tends to decrease. As a result, the AFM order was observed at underdoped IPs of Tl1245 ($n=5$) with $T_N=45$ K and an AFM moment of $M_{\text{AFM}} \sim 0.1\mu_B$. The most important outcome from this result is evidence

that the AFM order at each IP coexists uniformly below $T_N=45$ K with the SC state below $T'_c=87$ K.^{3,7} Further reduction of the hole density in the series results in the uniform coexistence of AFM and SC orders even at an OP where $p(\text{OP})$ is less than the critical hole density p_c for the onset of AFM order.^{3,4,8} Regarding the n dependence of p_c , previous works revealed that as n increases from $n=3$ to 4 to 5, $p_c(n)$ increases from 0.075 to 0.08 to 0.10,^{3,4} which demonstrates that the interlayer magnetic interaction $J_{\text{out}}(n)$ becomes stronger with increasing n . It is noteworthy that once an AFM order emerges, M_{AFM} is dependent on the doping level p but independent of n , whereas T_N depends on n or $J_{\text{out}}(n)$. These results have enabled us to present the ground-state phase diagram of SC and AFM orders as a function of the hole doping level for the multilayered cuprates with $3 \leq n \leq 5$ and to compare it with the theoretically deduced phase diagrams for 2D doped Mott insulators.^{3,4}

In this Letter, we report on ⁶³Cu- and ²⁰⁵Tl-NMR studies of the six-layered cuprate Tl1256 with $T_c \sim 100$ K, which provide evidence that an AFM order takes place below $T_N \sim 170$ K. In the homologous series of Tl12($n-1$) n ($n \leq 6$) in the optimally doped regime, we find that T_N is four times larger for $n=6$ than for $n=5$, whereas no trace of AFM order was observed for $n \leq 4$. This is considered to be because $J_{\text{out}}(n)$ for $n=6$ is significantly larger than that for $n=5$. Since T_c for both compounds is almost the same, we remark that even in the multilayered cuprates, the SC order is mostly dominated by the long-range in-plane SC correlation, which is insensitive to the magnitude of T_N and AFM moments at the IPs. This is the unique interplay between the high- T_c SC and AFM orders observed in the six-layered cuprates.

*E-mail: mukuda@mp.es.osaka-u.ac.jp

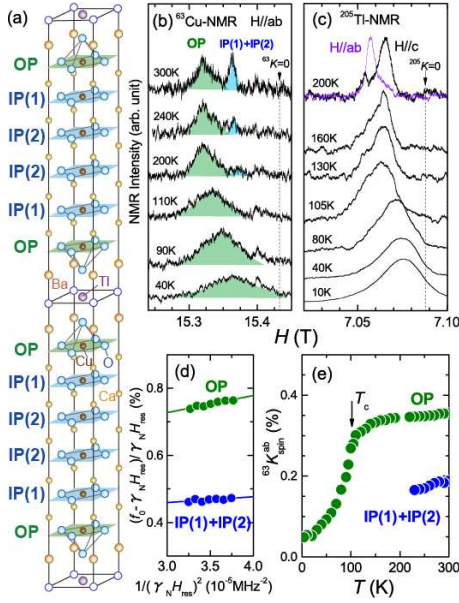


Fig. 1. (color online) (a) Crystal structure of six-layered Tl1256, which includes three inequivalent CuO_2 layers denoted as OP, IP(1), and IP(2). T dependences of (b) ^{63}Cu -NMR and (c) ^{205}Tl -NMR spectra. (d) Plot of $(f_0 - \gamma_N H_{\text{res}})/\gamma_N H_{\text{res}}$ against $1/(\gamma_N H_{\text{res}})^2$ from Eq. (1). The slope gives the value of ν_Q . (e) T dependence of $^{63}K_s^{\text{ab}}(T)$ for OP and IPs. Here, the data at IP(1) and IP(2) are not resolved, presumably due to similar values of the Knight shift and ν_Q .

A polycrystalline sample of $\text{TlBa}_2\text{Ca}_5\text{Cu}_6\text{O}_{14+\delta}$ (Tl1256) was synthesized under an appropriate pressure and temperature.⁹ The lattice parameters were $a=3.846$ Å and $c=25.380$ Å, determined by powder X ray diffraction. T_c was evaluated to be 100 K from the onset of a sharp diamagnetic signal in the dc susceptibility. For the NMR measurements, we used oriented powder samples aligned along the c -axis under a high magnetic field of $H_0=15$ T. The ^{63}Cu - and ^{205}Tl -NMR spectra were obtained at a frequency of $f_0=174.2$ MHz by sweeping an external field perpendicular or parallel to the c -axis. The present NMR results for Tl1256 ($n=6$) completely differ from those reported thus far for the compounds with $n \leq 5$, although it is not completely ruled out that a negligible amount of impurity phases such as Tl1245($n=5$) are contaminated in the sample preparation process.

Figure 1(b) indicates the temperature (T) dependence of the ^{63}Cu -NMR spectrum for the central transition ($+1/2 \leftrightarrow -1/2$). Since the NQR frequency ν_Q of ^{63}Cu (nuclear spin $I=3/2$) is sufficiently smaller than the Zeeman field, the central peak for the NMR spectrum ($+1/2 \leftrightarrow -1/2$ transition) is shifted by the second-order perturbation of the nuclear quadrupole interaction. In the case that an external field is applied perpendicular to the c -axis, the following relation is valid:

$$\frac{f_0 - \gamma_N H_{\text{res}}}{\gamma_N H_{\text{res}}} = K^{\text{ab}} + \frac{3\nu_Q^2}{16(1 + K^{\text{ab}})} \frac{1}{(\gamma_N H_{\text{res}})^2}, \quad (1)$$

where f_0 is the NMR frequency, γ_N the nuclear gyromagnetic ratio of a Cu nucleus, H_{res} the NMR resonance field, ν_Q the nuclear quadrupole frequency, and K^{ab} the Knight shift for $H \perp c$. As shown in Fig. 1(d), the slope

of the plot of $(f_0 - \gamma_N H_{\text{res}})/\gamma_N H_{\text{res}}$ against $1/(\gamma_N H_{\text{res}})^2$ gives the value of ν_Q at the IPs and OP. The estimated values of $^{63}\nu_Q=9.7$ and 16.6 MHz allow us to assign the two peaks in the spectra of Fig. 1(b) to the IPs and OP, respectively, since the similar values of $^{63}\nu_Q$ have been reported for the IPs and OP previously.⁶ Note here that, as shown in Fig. 1(a), the four IPs include two inequivalent IPs, IP(1) and IP(2), but it is not possible to resolve each spectrum associated with IP(1) and IP(2) owing to their comparable values of ν_Q .

Figure 1(e) indicates the T dependence of the spin component of the ^{63}Cu Knight shift $^{63}K_s^{\text{ab}}$, which is evaluated by subtracting the orbital part of the Knight shift $^{63}K_s^{\text{orb}} \sim 0.21(\pm 0.01)\%$ from K^{ab} . The marked decrease in $^{63}K_s^{\text{ab}}$ below T_c reveals the decrease in the spin susceptibility owing to the formation of a spin-singlet Cooper pairing. The empirical relationship between the hole density p and the value of $^{63}K_s^{\text{ab}}$ at 300 K¹⁰ enables us to evaluate $p(\text{OP})$ to be ~ 0.152 and $\bar{p}(\text{IPs})$ to be ~ 0.076 . Here, the $\bar{p}(\text{IPs})$ represents the average value of $p[\text{IP}(1)]$ and $p[\text{IP}(2)]$. Provided that p at each CuO_2 plane follows the spatial dependence of the Madelung potential from the apical oxygen O^{2-} [see Fig. 2(d)], the relation $p(\text{OP}) > p[\text{IP}(1)] > p[\text{IP}(2)]$ is expected and $p[\text{IP}(1)] \sim 0.086$ and $p[\text{IP}(2)] \sim 0.07$ are tentatively estimated using $p(\text{OP})=0.152$. The average value $\bar{p}(\text{IPs})$ of $p[\text{IP}(1)]$ and $p[\text{IP}(2)]$ almost coincides with $\bar{p}(\text{IPs}) \sim 0.076$ extracted experimentally from K^{ab} . As possible evidence for the AFM order at IPs, we note that the Cu-NMR spectra at the IPs disappear below ~ 200 K owing to the development of AFM correlations upon cooling toward T_N , but the Cu-NMR spectrum at the OP is observable down to low temperatures, suggesting that the OP does not play a primary role in the onset of AFM order.

Zero-field Cu-NMR/NQR measurements were performed at 1.8 K for Tl1256($n=6$) to gain an insight into the AFM ordered state. Figure 2 indicates the NMR spectra for (a) Tl1256, (b) Tl1245($n=5$) with $T_c=100$ K,³ and (c) Tl1223($n=3$) with $T_c=133$ K. The nuclear Hamiltonian \mathcal{H}_N for the Cu nucleus ($I=3/2$) at zero external field is described in terms of the Zeeman interaction $\mathcal{H}_Z = -\gamma_N \hbar \mathbf{H}_{\text{int}} \cdot \mathbf{I}$ and the nuclear quadrupole interaction $\mathcal{H}_Q = (\hbar \nu_Q/2)(I_z^2 - 5/4)$, where H_{int} is the internal field at the Cu site induced by AFM moments. In the case that the IPs and OP are in the nonmagnetic state with $H_{\text{int}}=0$, the Cu-NQR spectra should be observed at $^{63}\nu_Q(\text{IPs}) \sim 9.7$ and $^{63}\nu_Q(\text{OP}) \sim 16.6$ MHz, as shown by the dotted lines in Fig. 2. As a matter of fact, such the spectra are observed in Fig. 2(c) for Tl1223($n=3$), which does not have an AFM order. Accordingly, the spectrum with a peak at ~ 16 MHz in Fig. 2(a) is assigned to the OP, which is in the paramagnetic state. For the IPs, the peaks around ~ 25 and 42 MHz in the spectra are assigned to IP(1) and IP(2), respectively, revealing that both are in the AFM ordered state. This is because these frequencies are much higher than $^{63}\nu_Q(\text{IPs}) \sim 9.7$ MHz, pointing to the presence of an internal field H_{int} at the IPs. In fact, on the basis of the nuclear Hamiltonian of $\mathcal{H}_N = \mathcal{H}_Z + \mathcal{H}_Q$, a simulation of these spectra gives $H_{\text{int}}=2.1$ and 3.6 T for IP(1) and IP(2), respectively. Using the relation $H_{\text{int}}=|A_{\text{ab}} - 4B|M_{\text{AFM}}$, spon-

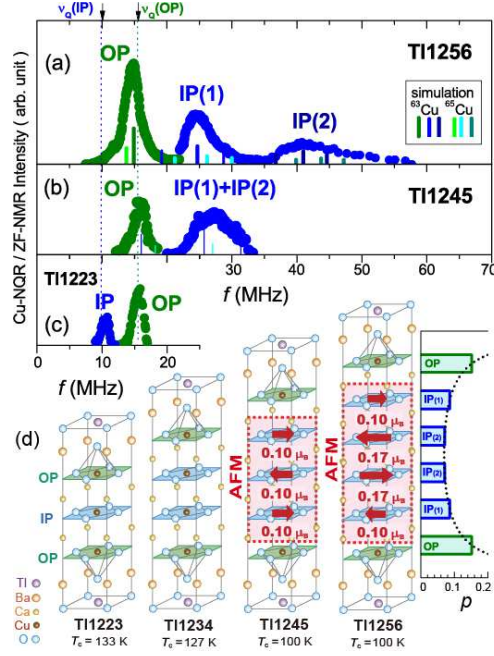


Fig. 2. (color online) Zero-field Cu-NMR/NQR spectra of Tl12($n-1$) n at 1.8 K for (a) $n=6$, (b) $n=5$ ($T_c=100$ K),³ and (c) $n=3$ ($T_c=133$ K). The solid bars in (a) and (b) are simulated resonance frequencies and intensities for the two isotopes ^{63}Cu and ^{65}Cu (see text). Dotted lines represent typical NQR frequencies ($^{63}\nu_Q$) in the case that the IPs and OP are in the nonmagnetic state. (d) Crystal structure of Tl12($n-1$) n with $3 \leq n \leq 6$, schematic views of the AFM order at 1.8 K for $n \geq 5$, and the distribution of the hole density at each layer for $n=6$.

taneous AFM moments of $M_{\text{AFM}}(\text{IP}(1))=0.10\mu_B$ and $M_{\text{AFM}}(\text{IP}(2))=0.17\mu_B$ are estimated at $T=1.8$ K, as illustrated schematically in Fig. 2(d). Here, we assume that the on-site hyperfine field is $A_{ab} \approx 3.7$ T/ μ_B , the transferred hyperfine field from the nearest-neighbor Cu site is $B(\text{IP}) \approx 6.1$ T/ μ_B , and $B(\text{OP}) \approx 7.4$ T/ μ_B .⁶ As a result, the AFM order with $M_{\text{AFM}}(\text{IP}(1))=0.10\mu_B$ and $M_{\text{AFM}}(\text{IP}(2))=0.17\mu_B$ emerges at the respective hole densities of $p(\text{IP}(1)) \sim 0.086$ and $p(\text{IP}(2)) \sim 0.07$. We highlight the fact that the present relationship between M_{AFM} and p in Tl1256($n=6$) coincides with the ground-state phase diagram of the SC and AFM orders as a function of p for the multilayered cuprates with $3 \leq n \leq 5$,³ ensuring that this phase diagram is independent of n .

Here, we show the ^{205}Tl -NMR results at the CRL, which enable us to gain an insight into the 3D magnetic interaction J_{CRL} among the inter-unit-cells through the CRL and determine T_N . Figure 1(c) shows the T dependence of the ^{205}Tl -NMR spectra. The spectra for $H\parallel c$ and $H\parallel ab$ (see the data at 200 K) are well resolved and the T dependences of ^{205}Tl Knight shift for $H\parallel c$ and $H\parallel ab$ are presented in Fig. 3(a). $^{205}K^{ab(c)}$ comprises the spin component $^{205}K_s^{ab(c)}$ and the T -independent orbital component $^{205}K_{\text{orb}}^{ab(c)}$.¹¹ $^{205}K_s^{ab(c)}$ is associated with an anisotropic hyperfine field supertransferred by the 6s- and 6p-spin polarizations at the Tl site, originating from the spin polarization at the IPs and OP. As shown in Fig. 3(a), the rapid decrease in $^{205}K^{ab(c)}$ below T_c is attributed to that in $^{205}K_s^{ab(c)}$ due to the

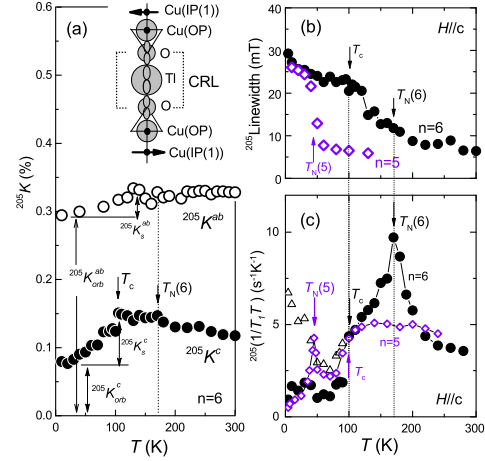


Fig. 3. (color online) (a) T -dependence of ^{205}Tl Knight shift for $H\parallel c$ and $H\parallel ab$. See the text for a description of the inset. T -dependences of (b) ^{205}Tl -NMR linewidth for $H\parallel c$ and (c) $^{205}(1/T_1T)$ for Tl1256 and Tl1245. The peaks of $^{205}(1/T_1T)$ indicate that $T_N=170$ and 45 K for Tl1256 and Tl1245, respectively. The open diamonds in (b) and (c) represent the ^{205}Tl -NMR data for Tl1245 with $T_c=100$ K and $T_N=45$ K.³

formation of spin-singlet Cooper pairs. Since $^{205}K_s^{ab(c)}$ approaches zero well below T_c , the values of $^{205}K^{ab}$ and $^{205}K^c$ at $T \ll T_c$ give ~ 0.29 and $\sim 0.07\%$, respectively. Furthermore, it is anticipated that the anisotropic spin part in the Knight shift exhibits $^{205}K_s^c > ^{205}K_s^{ab}$, suggesting that the dipole hyperfine field from the spin polarization at the $6p_z$ orbital is larger than those at the $6p_{x,y}$ orbitals. By contrast, the anisotropy in the orbital part exhibits $^{205}K_{\text{orb}}^c < ^{205}K_{\text{orb}}^{ab}$. In general, K_{orb} originates from the van Vleck susceptibility, which is proportional to $|\langle g|\mathbf{L}|e\rangle|^2/|\epsilon_g - \epsilon_e|$. Here, $\epsilon_g(|g\rangle)$ and $\epsilon_e(|e\rangle)$ denote the energies (wave functions) for the ground state and the excited states, respectively, and \mathbf{L} is the orbital angular momentum operator.¹² Provided that $6p_z$ and $6p_{x,y}$ are in the ground and excited states, respectively, it is expected that $^{205}K_{\text{orb}}^z \propto |\langle p_z|L_z|p_{x,y}\rangle|^2=0$ and $^{205}K_{\text{orb}}^{x,y} \propto |\langle p_z|L_{x,y}|p_{y,x}\rangle|^2>0$. As a result, the spin densities on the 6s and $6p_z$ orbitals at the Tl site are responsible for the anisotropy in the spin and orbital parts, playing a significant role in the interlayer magnetic coupling J_{CRL} through the possible covalency with the 4s and $3d_{x^2-y^2}$ orbitals of Cu via the $2p_z$ and $2s$ orbitals of apical O. This event is schematically drawn in the inset of Fig. 3(a). These microscopic outcomes resemble the previous ^{205}Tl -NMR results for single-layered Tl1201,^{11,12} indicating that the local electronic state at the Tl site, and hence J_{CRL} , does not vary from $n=1$ to 6.

Next, we estimate T_N from the measurements of $^{205}(1/T_1T)$. Its T dependence exhibits a peak at 170 K, as shown in Fig. 3(c). The distinct peak in $^{205}(1/T_1T)$ gives evidence that an AFM order occurs in a long-range manner. Below T_N , as shown in Fig. 3(b), the linewidth in the ^{205}Tl -NMR spectra starts to increase, similar to the case for Tl1245, giving another evidence for the onset of the AFM order. These similar behaviors were observed in the ^{205}Tl -NMR spectra of Tl1245($n=5$) at $T_N(5)=45$

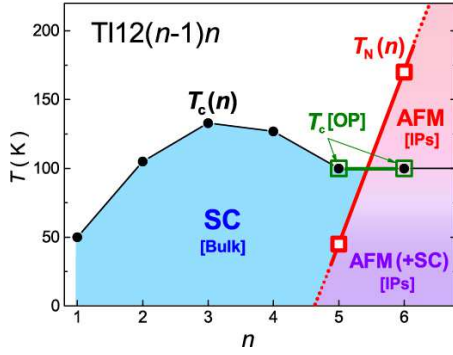


Fig. 4. (color online) Plots of $T_c(n)^{9,13}$ and $T_N(n)$ as functions of n for $\text{Tl}12(n-1)n$ in optimally doped regime. In this series, the AFM order appears at the IPs for $n \geq 5$. Previous studies on $n=5$ revealed that the AFM order at the IPs coexists uniformly below $T_N=45$ K with the SC state below $T_c'[\text{IPs}]=87$ K,^{3,7} enabling us to deduce that the ground state of the IPs of $n=6$ is the uniform coexistence of the AFM order with possible SC.

K, below which the underdoped IPs with $\bar{p} \sim 0.097$ shows the AFM order with $M_{\text{AFM}}(\text{IPs}) \sim 0.1 \mu_B$.³

Figure 4 presents plots of $T_c(n)^{9,13}$ and $T_N(n)$ for the homologous series of n -layered $\text{Tl}12(n-1)n$ in the optimally doped regime. In this series, the AFM order appears at the IPs for $n \geq 5$ but not for $n \leq 4$. The marked increases in $T_N(n)$ and $M_{\text{AFM}}(n)$ from $n=5$ to 6 are considered to be associated with the increase in the interlayer magnetic coupling $J_{\text{out}}(n)$. Note that when the total charge of the CRL is significantly reduced in the multilayered cuprates with apical fluorine, the AFM order appears for $n=3$ and 4.^{14,15} $M_{\text{AFM}}(n)$ at the AFM IPs in these compounds is much smaller than $0.5 \mu_B$ in the Mott insulator $\text{CaCuO}_2(n=\infty)$,² since it is uniformly reduced by the mobile holes with $p(\text{IPs})$, which are responsible for the onset of SC order in the AFM *metallic* state. Here, we should emphasize that the AFM order at each IP in $\text{Tl}1245(n=5)$ coexists uniformly below $T_N=45$ K with the SC state below $T_c'[\text{IPs}]=87$ K,^{3,7} enabling us to deduce that the AFM order at the IPs of $\text{Tl}1256(n=6)$ also coexists with the possible SC order inherent to the IPs in the ground state.

On the other hand, $T_c \sim 100$ K is maintained for $n=5$ and 6; nevertheless, $T_N(6)$ ($T_N(5)$) is significantly larger (smaller) than the bulk T_c . Here, it is interesting that $T_c \sim 100$ K for $n=5$ and 6 is also comparable with that for optimally doped single-layered Hg-1201 , indicating that the SC order parameter for $n=5$ and 6 is mostly dominated by the hole density at the optimally doped OP and the in-plane SC correlation. This is in contrast to the case of $n=3$, where a higher T_c (~ 133 K) is realized at three SC layers where the charge imbalance between the IP and OP is quite small.⁵ Note that the SC Cooper pairs in $n=6$ can tunnel between the OP through the AFM IPs by Josephson coupling as predicted in a theoretical study of multilayered cuprates.¹⁶ In this context, we suggest that the possible interlayer Josephson coupling between the AFM IPs and the OP is insensitive to the magnitude of T_N and the AFM moments at the IPs or the AFM interaction among the IPs, demonstrating a novel interplay between the SC and AFM orders at $n \geq 5$,

where the charge imbalance between the IP and OP is significantly large.

In summary, site-selective ^{63}Cu -NMR/NQR and ^{205}Tl -NMR studies on six-layered $\text{Tl}1256$ with $T_c=100$ K have revealed that the AFM order with moments of 0.10 and $0.17 \mu_B$ takes place at the inner CuO_2 planes IP(1) and IP(2), respectively, below 170 K. This is the consequence of the underdoped hole densities at IP(1) and IP(2) with $p \sim 0.086$ and ~ 0.07 , respectively. We highlight the fact that the increase in the out-of-plane magnetic interaction within the intra-unit-cell causes $T_N(5) \sim 45$ K for $\text{Tl}1245$ with $n(\text{IP})=3$ to increase to $T_N(6) \sim 170$ K for $\text{Tl}1256$ with $n(\text{IP})=4$, whereas no trace of AFM order was observed for $n \leq 4$. The interesting finding in this work is that the marked increases in T_N and AFM moments for the IPs do not bring about any reduction in T_c , since $T_c \sim 100$ K is maintained for both the compounds with a nearly optimally doped OP. We remark that even in the multilayered cuprates, the SC order for $n \geq 5$ is mostly dominated by the long-range in-plane SC correlation, which is insensitive to the magnitude of T_N and the AFM moments at the IPs or the AFM interaction among the IPs, demonstrating the novel interplay between the SC and AFM orders at $n \geq 5$. This is in contrast to the case of $n=3$, for which a higher T_c (~ 133 K) is realized at the three SC layers, where the charge imbalance between the IP and OP is quite small.

This work was supported by JSPS KAKENHI Grant Nos. 26400356, 26610102, and 16H04013.

- 1) N. D. Mermin and H. Wagner, *Phys. Rev. Lett.* **17**, 1133 (1966).
- 2) J. M. Tranquada, in *Handbook of High-Temperature Superconductivity* (Springer, New York, 2007), p. 257.
- 3) H. Mukuda, S. Shimizu, A. Iyo, and Y. Kitaoka, *J. Phys. Soc. Jpn.* **81**, 011008 (2012).
- 4) S. Shimizu, S.-i. Tabata, S. Iwai, H. Mukuda, Y. Kitaoka, P. M. Shirage, H. Kito, and A. Iyo, *Phys. Rev. B* **85**, 024528 (2012).
- 5) H. Kotegawa, Y. Tokunaga, K. Ishida, G.-q. Zheng, Y. Kitaoka, K. Asayama, H. Kito, A. Iyo, H. Ihara, K. Tanaka, K. Tokiwa, and T. Watanabe, *Phys. Rev. B* **64**, 064515 (2001).
- 6) H. Kotegawa, Y. Tokunaga, Y. Araki, G.-q. Zheng, Y. Kitaoka, K. Tokiwa, K. Ito, T. Watanabe, A. Iyo, Y. Tanaka, and H. Ihara, *Phys. Rev. B* **69**, 014501 (2004).
- 7) H. Mukuda, Y. Yamaguchi, S. Shimizu, Y. Kitaoka, P. M. Shirage, and A. Iyo, *J. Phys. Soc. Jpn.* **77**, 124706 (2008).
- 8) H. Mukuda, M. Abe, Y. Araki, Y. Kitaoka, K. Tokiwa, T. Watanabe, A. Iyo, H. Kito, and Y. Tanaka, *Phys. Rev. Lett* **96**, 087001 (2006).
- 9) A. Iyo, Y. Tanaka, H. Kito, Y. Kodama, P. M. Shirage, D. D. Shivagan, H. Matsuhata, K. Tokiwa, and T. Watanabe, *J. Phys. Soc. Jpn.* **76**, 094711 (2007).
- 10) S. Shimizu, S. Iwai, S.-i. Tabata, H. Mukuda, Y. Kitaoka, P. M. Shirage, H. Kito, and A. Iyo, *Phys. Rev. B* **83**, 144523 (2011).
- 11) S. Kambe, H. Yasuoka, A. Hayashi, and Y. Ueda, *Phys. Rev. B* **48**, 6593 (1993).
- 12) O. M. Vyaselev, N. N. Kolesnikov, M. P. Kulakov, and I. F. Schegolev, *Physica C* **199**, 50 (1992).
- 13) B. A. Scott, E. Y. Suard, C. C. Tsuei, D. B. Mitzi, T. R. McGuire, B.-H. Chen, and D. Walker, *Physica C* **230**, 239 (1994).
- 14) S. Shimizu, S.-i. Tabata, H. Mukuda, Y. Kitaoka, P. M. Shirage, H. Kito, and A. Iyo, *Phys. Rev. B* **83**, 214514 (2011).
- 15) S. Shimizu, H. Mukuda, Y. Kitaoka, H. Kito, Y. Kodama, P. M. Shirage, and A. Iyo, *J. Phys. Soc. Jpn.* **78**, 064705 (2009).
- 16) M. Mori and S. Maekawa, *Phys. Rev. Lett.* **94**, 137003 (2005).